frontiers | Frontiers in Earth Science

ORIGINAL RESEARCH
published: 04 July 2022
doi: 10.3389/feart.2022.827933

Assessing Modern *Calluna* Heathland Fire Temperatures Using Raman Spectroscopy: Implications for Past Regimes and Geothermometry

Thomas Theurer[1]*, *Noemi Naszarkowski*[2], *David K. Muirhead*[1], *David Jolley*[1] and *Dmitri Mauquoy*[1]

[1]School of Geosciences, University of Aberdeen, Aberdeen, United Kingdom, [2]School of Biological Sciences, University of Aberdeen, Aberdeen, United Kingdom

Charcoal geothermometry continues to offer considerable potential in the study of palaeowildfires over decadal, centennial, millennial, and deep time scales—with substantial implications for the understanding of modern wildfire intensification. Recent developments in the application of Raman spectroscopy to carbonaceous organic material have indicated its capability to potentially reconstruct the palaeocharcoal formation temperature, and equivalent palaeowildfire pyrolysis intensity. Charcoal reflectance geothermometry (which also relies upon microstructural change with thermal maturation) has also been the subject of extensive modern evaluation, with multiple studies highlighting the key influence of energy flux on the resultant charcoal microstructure. The ability to accurately quantify modern wildfire temperatures based upon novel Raman-charcoal analyses has not yet been attempted. Using Raman band width-ratios (i.e., FWHMRa) and accompanying geothermometric trends to natural wildfire charcoals, our results identify differences between microstructurally-derived fire temperatures compared to those recorded during the fire event itself. Subsequent assessments of wildfire energy flux over time indicate no dominant influence for the observed differences, due to the inherent complexity of natural fire systems. Further analysis within this study, regarding the influence of reference pyrolysis methodology on microstructural change, also highlights the difficulty of creating accurate post-fire temperature reconstructions. The application of Raman spectroscopy, however, to the quantification of relative changes in fire temperature continues to prove effective and insightful.

Keywords: charcoal, raman spectroscopy, geothermometry, wildfire, microstructure, organic carbon, pyrolysis

OPEN ACCESS

Edited by:
Samuel Abiven,
University of Zurich, Switzerland

Reviewed by:
Jun Inoue,
Osaka City University, Japan
Scott David Mooney,
University of New South Wales, Australia

***Correspondence:**
Thomas Theurer
t.theurer.19@abdn.ac.uk

Specialty section:
This article was submitted to Biogeoscience, a section of the journal Frontiers in Earth Science

Received: *02 December 2021*
Accepted: *10 June 2022*
Published: *04 July 2022*

Citation:
Theurer T, Naszarkowski N, Muirhead DK, Jolley D and Mauquoy D (2022) Assessing Modern Calluna Heathland Fire Temperatures Using Raman Spectroscopy: Implications for Past Regimes and Geothermometry. Front. Earth Sci. 10:827933. doi: 10.3389/feart.2022.827933

1 INTRODUCTION

A significant shift in global fire regimes—characterized by greater duration, intensity and atypical seasonality–has instigated fresh and serious consideration for the role of anthropogenic climate change on the future of fire (e.g., Phillips and Nogrady, 2020) as we enter the "Pyrocene" (Pyne, 2015). Studies into the understanding of palaeowildfires—those occurring over decadal, centennial, millennial, and deep time scales—have often focused on the assessment of the driving forces behind

changes in wildfire intensity, for example, climatic, atmospheric oxygen, and ecosystem fluctuations (Scott, 1989). Considerable insight has been drawn into the interactions between fire, palaeobotany and palaeoclimate throughout the early Palaeozoic (e.g., Edwards and Axe, 2004; Glasspool et al., 2004; Glasspool et al., 2006; Rimmer et al., 2015), late Palaeozoic (e.g., Nichols and Jones, 1992; Scott and Jones, 1994; Jasper et al., 2013; Benicio et al., 2019), Mesozoic (e.g., Harris, 1958; Belcher et al., 2010; Belcher and Hudspith, 2016a; Zhang et al., 2020) and into the Cenozoic (e.g., Keeley and Rundel, 2005; Zhou et al., 2014; Korasidis et al., 2016). Studies into recent sediment records have focused significantly upon the role of humans in utilising fire and modifying environments, often with insights into anthropogenic climate change and its effects (Marlon et al., 2013). The analysis of fire during the Palaeocene-Eocene boundary (Collinson et al., 2007; Collinson et al., 2009; Denis et al., 2017) has proven particularly relevant to our modern situation, given similarities in the climatic thermal-maximum and projections of extreme anthropogenic climate change (McInerney and Wing, 2011; IPCC, 2021, p. TS-101).

Aside from the study of polycyclic aromatic hydrocarbons (PAHs) associated with palaeocombustion (e.g., Marynowski and Simoneit, 2009; Nabbefeld et al., 2010; Zakrzewski et al., 2020), assessing changes in wildfire activity through time is typically achieved through palaeowildfire-derived charcoal geothermometry. This refers to the quantification of palaeofire temperatures from the thermal conditions of charcoal and inertinite formation. Whilst this has been achieved historically and extensively by the application of charcoal reflectance (e.g., Edwards and Axe, 2004; Petersen and Lindström, 2012; Rimmer et al., 2015; Benicio et al., 2019), recent studies have introduced the application of Raman spectroscopy as a novel and effective method of charcoal geothermometry (Rouzaud et al., 2015; Deldicque et al., 2016; Deldicque and Rouzaud, 2020; Mauquoy et al., 2020; Theurer et al., 2021).

The thermal alteration of organic carbon and carbonaceous matter, including as a result of burial and coalification, has been extensively interpreted using Raman spectroscopy—often in conjunction with studies in vitrinite reflectance (Henry et al., 2019b *and references therein*). It has been shown that, with increasing temperature and often burial pressure, the microstructure of carbon in organic material undergoes a process of structural reorganization—varying in composition and proportion of amorphous carbon (Tuinstra and Koenig, 1970). Here, "microstructure" refers, primarily, to the carbon bonds and molecular arrangements that result from changes in constituent chemistry. Microstructural reorganization is presented as the preferential removal of amorphous carbon bonding, and the subsequent increasing development of graphitic structures, shown by gradual changes in D- (amorphous) and G- (graphitic) bands (Tuinstra and Koenig, 1970; Beny-Bassez and Rouzaud, 1985; Wopenka and Pasteris, 1993; Ferrari and Robertson, 2000). The process of charcoalification, by application of thermal energy to plant-based organic material, exhibits a similar microstructural development. Processes are, however, varied in their constituent biochemistry, and limited by temperatures experienced. Following the initial dehydration of material below 250°C, exceedance of this temperature initiates the thermal degradation of component molecules (e.g., lignin, cellulose, hemicellulose) into aromatic compounds (Braadbaart and Poole, 2008; Braadbaart et al., 2009). Complete aromatization occurs at ~400°C, at which point the microstructure of charcoal is dominated by large planar aromatic sheets (Braadbaart and Poole, 2008; Braadbaart et al., 2009). Pervasive growth of polyaromatic units during the microstructural reorganization of charcoal remains broadly consistent with aforementioned changes in amorphous carbon under thermal maturation. This relationship between increasing temperature and microstructural organization during charcoalification has been reported using Raman spectroscopy in several instances (Yamauchi et al., 2000; Yamauchi and Kurimoto, 2003; Kawakami et al., 2005; Paris et al., 2005; Ishimaru et al., 2007a; Ishimaru et al., 2007b, Manabe et al., 2007; Potgieter-Vermaak et al., 2011 *and references therein*), often permitting geothermometry (e.g., Beyssac et al., 2002; Wilkins et al., 2014; Wilkins et al., 2015; Rouzaud et al., 2015; Deldicque et al., 2016; Wilkins et al., 2018; Henry et al., 2019a; Henry et al., 2019b; Deldicque and Rouzaud, 2020). Whilst the principles of carbonaceous structural reorganization are consistent, the Raman spectral response, associated parameters, and its derivation of the temperature-structure relationship depend on the regime of maturation and organic material under study (Henry et al., 2019b *and references therein*).

Despite numerous applications of Raman spectroscopy to charcoal and amorphous organic matter, no investigation into the correlation between experimental charcoal thermometry and true wildfire temperatures has yet been attempted for Raman spectroscopic methods. The application of charcoal reflectance analyses to modern wildfire charcoals—with the intention of better understanding temperature, intensity, and severity—may be found within several examples (e.g., Scott et al., 2000; Hudspith et al., 2015; New et al., 2018; Belcher et al., 2021). Similarly, Fourier-Transform Infra-Red spectroscopy (FTIR) has shown considerable potential in understanding chemical and microstructural change in charcoals (e.g., Guo and Bustin, 1998; Ascough et al., 2020). This has developed into applications in the assessment of wildfire intensity and severity (Gosling et al., 2019; Constantine et al., 2021; Maezumi et al., 2021). Nonetheless, many studies continue to rely on an assumption of harmony between experimental and naturally observed temperature-microstructure relationships.

Recent research in charcoal reflectance has highlighted the innate variability of energy within a natural wildfire system, and the inapplicability of oven-based experimental pyrolysis in replicating the true charcoalification process (Belcher and Hudspith, 2016b; Hudspith and Belcher, 2017; Belcher et al., 2018). However, modern studies utilising more accurate forms of experimental pyrolysis (i.e., calorimetry) have yet to corroborate thermometric calculations with precise natural wildfire temperatures. Discrepancies in natural vs. experimental fire thermometry may also be perpetuated by variable environmental conditions, and the inter- and intraheterogeneity of fuels (Ishimaru et al., 2007a; Guedes et al., 2010). Furthermore, in the context of palaeowildfires,

the nature of archaeological and geological records with regards to charcoal suggest considerable potential for alteration of wildfire evidence, through diagenetic processes such as humification and oxidation (Cohen-Ofri et al., 2006; Braadbaart et al., 2009; Ascough et al., 2008; Ascough et al., 2010; Ascough et al., 2011a; Ascough et al., 2018; Ascough et al., 2020; de Sousa et al., 2020; Smidt et al., 2020), and taphonomic bias (Scott and Damblon, 2010 *and references therein*). Such natural variability, particularly with regards to the influence of energy flux may bring into question the validity of historic assessments of palaeowildfire temperature.

The importance, therefore, of understanding energy flux within natural fire systems and their concurrence with geothermometric techniques remains significant. This is complicated somewhat by the association of fire temperatures and intensity in historic palaeofire study. Fire intensity refers more specifically to the energy release that occurs during a wildfire event, with considerable evidence suggesting this may not be consistent with recorded temperatures (Keeley, 2009). Reference, therefore, to "intensity" alongside temperature-specific geothermometry reflects a considerable misnomer. As a result, we have endeavored to draw a distinction between applications of Raman spectroscopy to measures of intensity, dependent on energy, vs. "pyrolysis intensity", derived from geothermometry. The limitative nature of the palaeofire record prevents the accurate quantification of energy flux, in turn preventing measures of intensity. This has been countered by the implementation of pyrolysis intensity in recent assessments of palaeoecosystem change, as a reflection of temperatures experienced during the pyrolysis of plant material in wildfires (Hudspith et al., 2015). This in turn has been related to fire severity, a measure of post-fire ecosystem mortality. The correlation of energy-dependent intensity with severity (Keeley, 2009) confirms a broader applicability of pyrolysis intensity as a proxy for intensity, given key relationships between fire structure, fuel consumption, and recorded temperatures (Theurer et al., 2021 *and references therein*). The exploration, however, of associations between fire temperature, energy flux, and charcoal microstructure below offer a unique opportunity to investigate the relationship, if any, between intensity and pyrolysis intensity.

In this study we present the first consideration of the influence of reference charcoal pyrolysis on the application of charcoal geothermometry in natural heathland wildfire systems, using Raman spectroscopy. The focus, here, on utilising a heathland environment is supported by the modern prominence of fire within these, and similar, ecosystems. A relationship with fire has indeed persisted in biomass-accumulative environments—such as peatland and wetlands—throughout geological history, often comprising a significant proportion of preserved palaeofire evidence (Scott, 2000 *and references therein*). Modern practices in the artificial promotion of fire, within NW European *Calluna vulgaris*-rich heathland environments, offer a unique opportunity to test Raman-charcoal geothermometry within a controlled environment with considerable modern and palaeowildfire context. Our research also continues to emphasize the relationship between microstructural change in charcoal with thermal alteration, *via* the application of an inert-atmosphere tube furnace. These data contribute toward a further evaluation of the influence of experimental pyrolysis methodology on Raman spectra and derived parameters. We ultimately underline the complications that may arise from characterizing complex natural fire processes using laboratory techniques, and the implications these may have for palaeowildfire study.

2 MATERIALS AND METHODS

2.1 Prescribed *Calluna* Fire

Charred *Calluna vulgaris* (L.) Hull (ling heather, hereafter *Calluna*) stem samples analyzed within this study were collected from experimental ("prescribed") fires, conducted at Glensaugh Research Farm in the Grampian Highlands of Aberdeenshire, Scotland (56°55′ N, 2°33′ W).

On the 12th of April 2021, fires implemented as part of an additional distinct research project were conducted within an area consisting predominantly of *Calluna–Vaccinium myrtillus* dry heath vegetation (**Figure 1B**), overlying a thin peaty podzol. The weather during the experimental fires remained sunny with a gentle breeze, whilst relative humidity and air temperature approximated 40% and 6°C, respectively. Two replicate plots (15 × 15 m) separated by a distance of 2 km were utilized for sampling, constrained by surrounding fire breaks cut prior to ignition. Using a diesel-fueled knapsack sprayer, both plots were ignited upwind and burnt within 3 hours of each other.

Temperature profiles across both plots were measured using wireless K-type thermocouples and *Tinytag* Loggers (Gemini Data Loggers, United Kingdom). Temperatures were recorded at 5 s intervals for the duration of fire progression exceeding minimum recordable temperature. A total of five thermocouple-logger pairs were utilized across both areas, buried toward the center of each plot, and spaced approximately 2 m apart. Burial within the soil was conducted in such a way as to ensure the heat-determinant thermocouple tip protruded ~2 cm above the moss surface layer. In order to ensure maximum fire temperatures recorded were similarly experienced by *Calluna* samples utilized in this study, the tip of each thermocouple was placed within 1 cm of a *Calluna* stem, later sampled. Stems identified for measurement and sampling were selected according to width, and equivalent likelihood of survival during the fire. Immediately following extinguishment, *Calluna* stems directly adjacent to each thermocouple were collected and placed into separate, clean containers. Following burning, a single temperature logger was deemed faulty as considerably lower temperatures were recorded than expected (<200°C). The data from this logger and the sample related to it were therefore omitted from this study. Samples of *Calluna* for fuel moisture content (FMC) analyses were also collected independently, adjacent to thermocouples, within 1 h of burning and placed in tightly sealed aluminium containers. FMC samples were then oven dried for 48 h at 80°C, at which point mass loss recorded was deemed equivalent to moisture content. This yielded an average stem FMC of 74.4 and 78.0% for each plot, respectively.

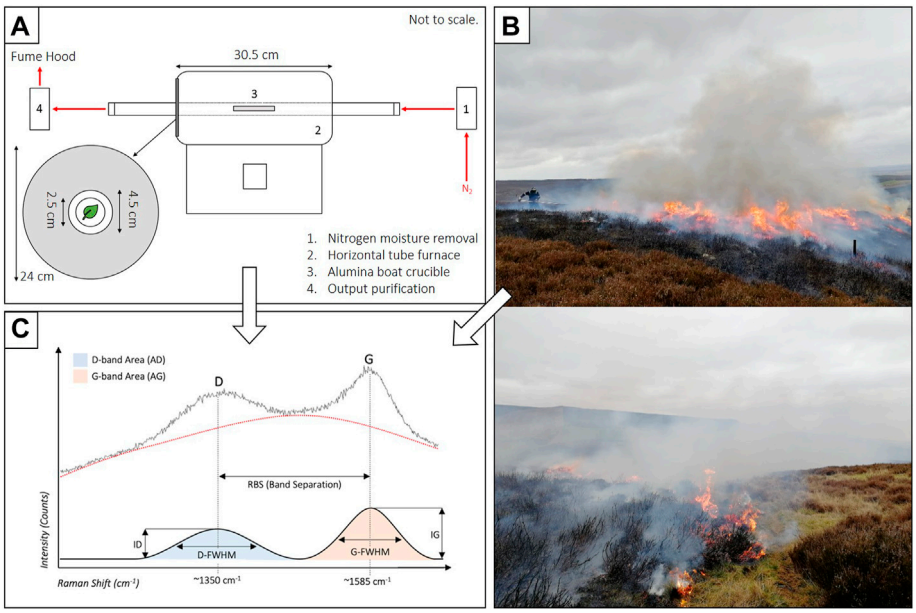

FIGURE 1 | A diagram highlighting the collective methodological components within this study, including; **(A)** a schematic representation of experimental pyrolysis using a tube furnace under an inert nitrogen atmosphere, **(B)** field photographs indicating conditions during, and propagation of, prescribed fire in the Glensaugh *Calluna* heathland, and **(C)** a representation of the method by which applied Raman parameters (labelled) are obtained *via* deconvolution, and their relationship to a raw spectrum (grey) and its baseline (red), *after* Theurer et al. (2021).

2.2 Tube Furnace Pyrolysis

Historically, the understanding of charcoal recorded in archive deposits has relied upon the generation of reference charcoals by the replication of pyrolysis in a laboratory (Orvis et al., 2005). Methods of pyrolysis—in lieu of natural fire processes—have included wrapping samples in foil, burying plant material in sand, and utilising an inert atmospheric furnace. Standard studies in charcoal geothermometry have utilized all of these methods at some time (e.g., Jones et al., 1991; Edwards and Axe, 2004; Scott and Glasspool, 2005; McParland et al., 2007; Ascough et al., 2010). This is contrasted by the reliance on inert atmospheric pyrolysis—often using a tube furnace—in Raman-charcoal analyses (e.g., Yamauchi et al., 2000; Yamauchi and Kurimoto, 2003; Paris et al., 2005; Zickler et al., 2006; Ishimaru et al., 2007a; Ishimaru et al., 2007b; Manabe et al., 2007; Deldicque et al., 2016; Deldicque and Rouzaud, 2020). Recent research, however, has determined that the use of laboratory furnaces to replicate natural wildfire conditions may not be appropriate. This is compared to more advanced techniques and equipment such as a calorimetry, or indeed, natural wildfires themselves (Belcher and Hudspith, 2016b; Hudspith and Belcher, 2017; Belcher et al., 2018). However, an assessment of methodological interference in the application of Raman spectroscopy to charcoals—experimental or natural—has never been approached. In order to understand the influence of charcoalification methodology on Raman spectroscopy of charcoals, pyrolysis of plant material in a tube furnace has also been tested here with the intention of comparing to results using an alternate method of laboratory pyrolysis.

In order to replicate pyrolysis in an inert atmosphere, five 10 mm (L) × 2–3 mm (D) sections of *Calluna* stem were heated in a *Lenton* horizontal tube furnace under a constant flow of nitrogen (80 ml/min ± 10 ml/min), contained within an *Almath* Alumina BS100 boat crucible (15 ml) measuring 100 mm × 21 mm × 14 mm. Samples of *Calluna* stem were collected in Aberdeenshire (NE Scotland) in October 2020. Stem samples were dried prior to charring in a *Gallenkamp* "Hotbox" oven at 70°C until a constant weight was achieved. This ensured samples were completely devoid of free moisture, and any impacts on charcoal microstructure as a result of "wet" pyrolysis were negated (Belcher and Hudspith, 2016b). Throughout the heating process, the nitrogen gas was first passed through a drying agent in order to remove any moisture that may have influenced the process of pyrolysis. Temperatures of 250, 400, 600, 800, and 1000°C were utilized, heating samples from room temperature at a rate of 5°C/minute, with a dwell time of 90 min. Following completion of dwell time, samples were allowed to cool to room temperature before collection. Between experiments, the crucibles used were cleaned using concentrated nitric acid to prevent potential contamination. A schematic display of the experimental set-up implemented during tube furnace pyrolysis is shown in **Figure 1A**.

2.3 Raman Spectroscopy

Spectra were collected by applying an Ar+ green diode (514.5 nm) to samples, using a Renishaw InVia Reflex Raman spectrometer at the University of Aberdeen. A ×50 objective lens, in conjunction with a *Leica* DMLM reflected light microscope, was used to focus the laser spot (~1–2 μm). Prior to sampling, the laser was calibrated against the in-house *Renishaw* spectrometer silicon

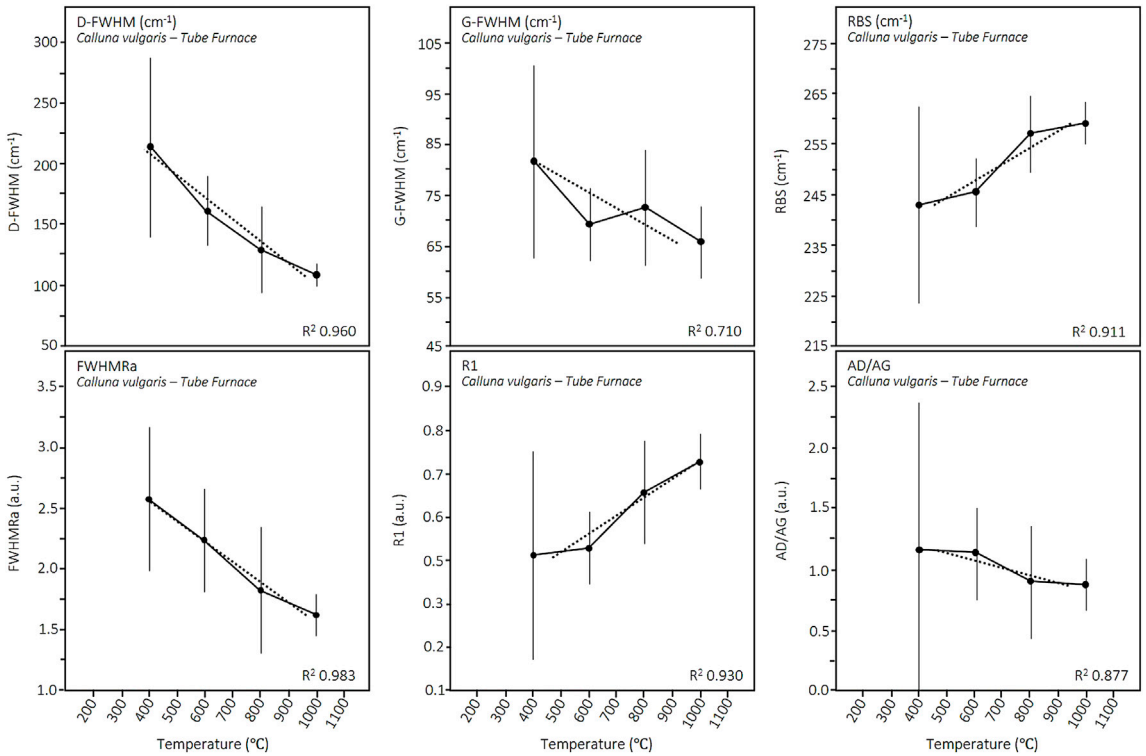

FIGURE 2 | Crossplots indicating the relationship between temperature of charcoal formation and Raman parameters—derived from tube furnace pyrolysis. Each data point reflects median values from 150 individual spectral deconvolutions, with standard deviations shown by vertical black lines. Linear trends are indicated by dotted grey lines, corresponding to R^2 values denoted in the bottom left corner of each crossplot.

sample. Manual crosshair and slit alignment calibration were completed where necessary. Upon sampling, spectra were recorded between 1100 and 1700 cm^{-1} and centered at 1400 cm^{-1} (3 cm^{-1} resolution). Per spectrum, three accumulations were recorded across a period of 15 s total (5 s per accumulation). *Renishaw* WiRE 3.0 Curve-fit software was implemented in the subsequent process of spectral deconvolution; consisting of smoothing, baseline extraction *via* cubic spline interpolation, and curve-fitting (**Figure 1C**). This process was implemented three times per acquisition, ensuring reproducibility and the removal of background interference. A laser power of 1% (<0.3 mW) was implemented to ensure spectra displayed a sufficient response, reduced fluorescence, and limited sample damage (Henry et al., 2018). Each charcoal sample—both experimental and naturally procured—was measured using the Raman spectrometer at ten randomly selected sampling points across five individual samples of charcoal, where possible. Charcoal sampling points were discerned and ultimately limited by microscopic identification of high surface reflectivity—indicating carbonaceous maturation associated with charcoalification.

Datasets acquired post-deconvolution were processed manually into the following Raman parameters; full-width at half-maximum of the D-band (D-FWHM) and G-band (G-FWHM), D- and G-band full-width at half-maximum ratio (FWHMRa, *formerly* D-FWHM/G-FWHM), D- and G-band peak separation (RBS), D- and G-band height ratio (R1), and D- and G-band area ratio (AD/AG). These parameters, and their relationship to the process of spectral deconvolution, are highlighted in **Figure 1C**.

3 RESULTS

3.1 Raman Parameters and Temperature—Tube Furnace Pyrolysis

Following deconvolution and the application of median values to parameter calculations—consistent with dataset non-normality ("Statistical Analyses")—trends detailed in **Figure 2** indicate the nature of temperature and spectral change in tube furnace-pyrolyzed charcoals. Due to the lack of spectra suitably displaying D- and G-bands at 250°C, this experimental temperature was not utilized in later assessments of trend for Raman parameters.

3.1.1 Full-Width at Half-Maximum Analyses (G-FWHM, D-FWHM, FWHMRa)

Analysis of parameters associated with FWHM (full-width at half-maximum) indicate that inverse proportionality—reduction of band width with increasing temperature—can be expected during the thermal maturation of charcoal in a tube furnace. D-FWHM and FWHMRa both indicate a strong linear relationship with temperature, though the width ratio displays

the strongest linearity of all parameters (R^2 0.983), compared to D-FWHM (R^2 0.960). Deviations from total linearity are indicated by reductions in trend gradient between 600 and 1000°C. This reduction in gradient is replaced by an inversion in trend for G-FWHM, resulting in the lowest linearity with temperature of all tested parameters (R^2 0.710). Standard deviation (indicated by error bars in **Figure 2**) appears to reduce with increasing experimental temperature for all FWHM-associated parameters, contradicted only by increases in standard deviation at 800°C, relative to 600°C. In all parameters, standard deviation at the 400°C production temperature is considerable.

3.1.2 Height and Area Ratios (R1, AD/AG), and Band Separation (RBS)

Similar to FWHM-associated parameters, AD/AG (band area ratio) displays inverse proportionality with increasing temperature, with variation in trend resulting in a near-linearity for AD/AG (R^2 0.877). In contrast, R1 (peak height, or "intensity", ratio) is one of two parameters displaying a direct relationship, increasing with temperature under strong linearity (R^2 0.930). The relationship between R1 and temperature is marked by a sharp increase in values between 600 and 800°C, followed by a lessened gradation in trend up to 1000°C. Band separation, alike R1, shows a near-linear (R^2 0.911) direct relationship with increasing formation temperature. **Figure 2** shows that RBS values increase more significantly between 600 and 800°C, resulting in an increase in trend gradient between these temperatures. Standard deviations indicate a similar pattern to those aforementioned within FWHM-associated parameters.

3.2 Raman Parameters and Temperature—Prescribed *Calluna* Fire

During experimental fire treatment of natural Scottish heathland ("Prescribed *Calluna* Fire"), thermocouple recordings indicated that each of the four *Calluna* sample sites were exposed to maximum temperatures of 466, 592, 705, and 803°C, respectively. Subsequent to spectroscopic study of charcoals from each of the sample sites, these maximum fire temperatures will be used to correlate calculations of Raman-derived thermal maturity (see below).

3.2.1 Full-Width at Half-Maximum Analyses (G-FWHM, D-FWHM, FWHMRa)

Investigation of Raman parameters associated with band width interactions in naturally derived *Calluna* charcoals indicates a consistent response to increasing maximum recorded flame temperature (MRFT *henceforth*). Median values in both D-FWHM and G-FWHM, as well as FWHMRa indicate no distinct linear trend with temperature (**Figure 3**). This appears to be the result of a significant inversion in trend at 705°C_{MRFT}, shifting toward higher width and ratio values typically indicative of lower thermal maturity. If this point is temporarily discounted, a general trend of reducing width with increasing temperature may be observed up to 592°C_{MRFT}, with a slight inversion at 803°C_{MRFT} toward higher values. The trend displayed in D-FWHM is notably comparable to typical values displayed in tube furnace pyrolysis between 466 and 592°C_{MRFT}. FWHMRa, in contrast, displays lower values at lower temperatures, followed by an inversion to higher values between 592 and 705°C_{MRFT}, relative to the trend displayed by tube furnace pyrolysis samples (**Figure 2**).

3.2.2 Height and Area Ratios (R1, AD/AG), and Band Separation (RBS)

As with band width parameters, RBS displays significant inversion at 705°C_{MRFT}, resulting in little difference between values for 466 and 705°C_{MRFT}, and 592 and 803°C_{MRFT} respectively. RBS values derived from 466°C_{MRFT} are similar to those values derived from tube furnace pyrolysis between 400 and 600°C, and a derivation of trend may indeed determine similar temperatures of formation between the two sources. In contrast to the median D-FWHM and G-FWHM results; RBS, AD/AG and R1 typically show values that are lower than those displayed by charcoals produced in tube furnace pyrolysis, with the exception of 466°C_{MRFT} in RBS (**Figure 3**). This highlights a further complexity in the results, with lower R1 and RBS typically associated with lower temperatures, and higher temperatures in AD/AG as shown in tube furnace trends. Nonetheless, R1 and AD/AG both indicate very little difference in values between 466 and 803°C_{MRFT}, with a slight inversion in R1 at 705°C_{MRFT} toward lower values.

3.3 Statistical Analyses

Assessments of distribution for both experimental (tube furnace) and natural (prescribed fire) charcoal results indicate non-normal distributions of the applied Raman parameters. Minor exceptions to this are found, inconsistently, within parameters R1, AD/AG, RBS. Subsequent one-way ANOVA, Levene's (standard and modified), and Welch's unequal-variance testing suggest, within each respective dataset, statistically significant variation between mean parameter values across all tested temperatures. Statistically significant heterogenous variance was recorded for parameter R1, derived from the prescribed fire dataset. For further information regarding applied statistical analyses - including tabulated results—**Supplementary Table S1**.

3.4 Geothermometric Application

3.4.1 Experimental Derivation and Results

In order to assess the ability for Raman geothermometry to characterize true wildfire temperatures accurately and consistently from charcoal microstructure, we have implemented FWHMRa to charcoals collected in a prescribed *Calluna* heathland fire. Suitable application of FWHMRa to the assessment of wildfire charcoal formation temperatures—as recommended in Theurer et al. (2021)—is corroborated by increased linearity within this study (**Figure 2**). A geothermometric equation has been derived from the linear trend displayed by FWHMRa, generated under tube furnace pyrolysis within this study (**Figure 2**). This equation is highlighted below (**Eq. 1**). As non-normality was typically exhibited in Raman results yielded from our natural *Calluna* wildfire samples (**Table 2** in **Supplementary Table S1**) the equation below has been applied to both median and mean

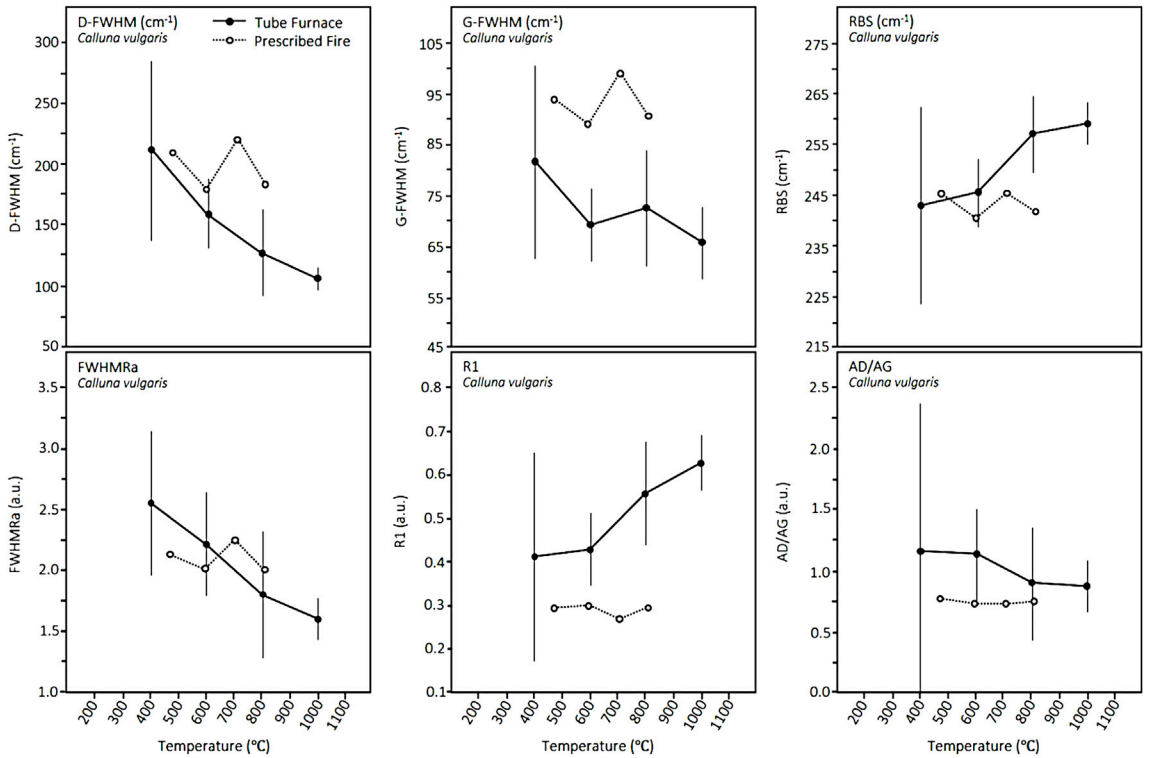

FIGURE 3 | Crossplots indicating the relationship between median Raman parameter values and the formation temperature of charcoals derived from prescribed fire (dashed black line, open circle) and tube furnace pyrolysis (black line, filled circle), respectively. Each data point reflects median values from 150 individual spectral deconvolutions, with standard deviations for the experimentally pyrolyzed charcoal dataset shown by vertical black lines. Key in top left crossplot corresponds to all succeeding plots.

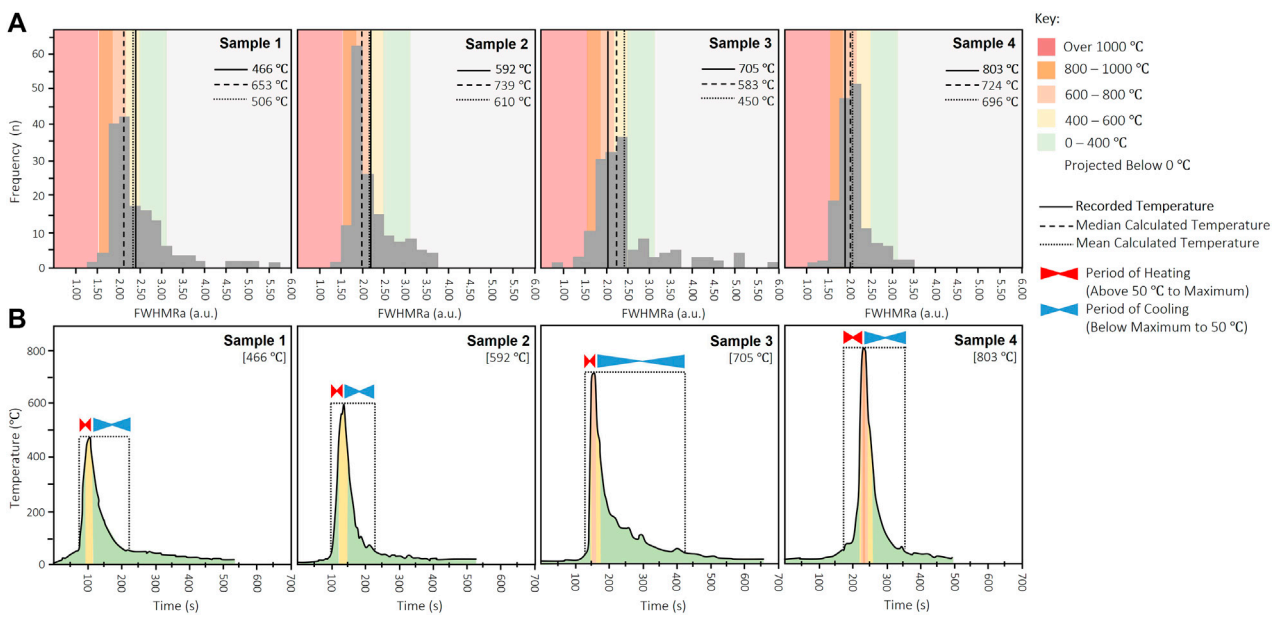

FIGURE 4 | Comparative diagrams corresponding to prescribed fire geothermometry, presenting; **(A)** the nature of Raman data distribution for each sample set, relative to the expected versus mean and median FWHMRa values, and **(B)** flame time-temperature plots denoting periods within certain temperature thresholds, and the cooling/heating periods relevant to these.

TABLE 1 | Table indicating the total duration of heating for each prescribed fire sample set, including the time taken to reach, and cool from, maximum recorded temperature. Heating rate and cooling rate are also highlighted. All values are presented to three significant figures, and considered strictly approximate given the recording capabilites and resolution of implemented thermocouples. Durations of heating are derived from times recorded immediately before and after 50°C is measured, and therefore may include lower temperatures than 50°C depending on the rate of increase between measurements. Values at 466°C_{MRFT} do not correspond to the recorded total duration as a result of the sustaining of maximum recorded temperature for 3 s.

Sample Set	Approximate duration of heating (s)			Heating rate (°C. s^{-1})	Cooling rate (°C. s^{-1})
	Total (>50°C)	50°C—Maximum	Maximum—50°C		
466°C_{MRFT}	168	39	126	10.8	3.33
592°C_{MRFT}	130	40	90	14.0	6.06
705°C_{MRFT}	250	25	225	26.8	2.93
803°C_{MRFT}	180	60	120	12.6	6.34

parameter values, with the intention of assessing the nature of data distribution. Understanding the effect of distribution on Raman-calculated temperatures may offer further insight into the interaction between maximum flame and typical charring temperature. The application of the geothermometric equation below, and the comparison between maximum recorded flame temperature and Raman-calculated temperature, are highlighted in **Figure 4**.

$$Formation\,Temperature\ (℃) = \frac{[FWHMRa] - 3.1765}{-0.0016} \quad (1)$$

Representing the spread of data relative to calculated and recorded fire temperatures, histograms for each sample set are shown in **Figure 4A**. These primarily highlight a reduction in data spread (i.e., presence of outlying data) with increasing temperature. The single exception to this is seen within samples generated at 705°C_{MRFT}. Values denoted by vertical lines in **Figure 4A** indicate the expected equivalent, mean, and median FWHMRa values associated with each sample set. Whilst median FWHMRa values and the temperatures derived from them are not wholly dissimilar from thermocouple recordings, percentage variation from the recorded temperature ranges between 9–40%. Mean values may generate temperatures close to those expected for samples at 466 and 592°C_{MRFT}, however significant deviation from this at higher temperatures, particularly for 705°C_{MRFT}, indicates the influence of outlying data on our proposed geothermometry. Within these data a pattern emerges. Namely, lower formation temperatures (466 and 592°C_{MRFT}) generate mean and median calculated values higher than those expected, exceeding recorded fire temperatures. In contrast, higher formation temperatures (705 and 803°C_{MRFT}) present the opposite relationship. This inversion in relationship between expected and calculated fire temperatures suggests a likewise inversion in the response of microstructure to temperature that cannot be explained solely by Raman parameters.

3.4.2 Time-Temperature Interactions

To better understand the variable disparity between recorded and calculated fire temperatures in the heathland fire, we have collected and utilized thermocouple recordings—indicating changes to fire temperature over time within each sample site (**Figure 4B**). Quantitative assessment of time-temperature curves (**Table 1**), indicate that 705°C_{MRFT} samples underwent the most overall time heated above 50°C, followed by 466 and 803°C_{MRFT}. Charcoal generated at 592°C_{MRFT} exhibited the shortest duration of heating. Our results also indicate that the sample set at 705°C_{MRFT} underwent the most rapid heating rate, alongside the slowest post-maximum cooling rate. Heating rates for 466, 592, and 803°C_{MRFT} remain relatively similar, whilst samples at 592 and 803°C_{MRFT} experienced a much faster cooling rate compared to 466°C_{MRFT}, and indeed, 705°C_{MRFT}.

Assessments of total energy (**Table 2**), as a function of area-under-curve measurements (e.g., Belcher et al., 2021), may also offer further insight into energy fluxes undergone during each *Calluna* heathland fire regime. This method of approximating energy change within a fire system relies on the relationship between energy exhibited by a fire system, and net change in temperature (°C) over time. By considering energy output above and below the key threshold of charcoalification (>300°C) we may better characterize the proportion of energy implemented in the development and maturation of charcoal microstructure.

As shown in **Table 2**, the fire system for 705°C_{MRFT} produced the most energy (equal to total °C) across the duration of heating above 50°C. This was followed by 803°C_{MRFT}, whilst the total energy for 466°C_{MRFT} and 592°C_{MRFT} systems remained similarly lower in intensity. Considering key approximate thermal thresholds of mortality (~50–299°C) and charcoalification and maturation (>300°C), **Table 2** indicates that both 803°C_{MRFT} and 705°C_{MRFT} exhibited the highest output of energy during an exceedance of 300°C. Below 300°C however, sample set 705°C_{MRFT} also expended the greatest amount of energy. The remaining samples all generated between 11800 and 15700 (°C) below 300°C, with the highest output in samples 466°C_{MRFT}, followed by 803°C_{MRFT} and 592°C_{MRFT}, respectively. More specifically, fire system 705°C_{MRFT} exhibited the greatest amount of energy out of all four sites within the ranges of 50–299°C and 300–399°C. The greatest energy produced above 400°C occurred at sample site 803°C_{MRFT}. In contrast, the 592°C_{MRFT} regime expended the least amount of energy between 50—299°C and 300–399°C, whilst 466°C_{MRFT} experienced the lowest total energy >400°C.

These results are not unexpected given the relationship between heightened temperature and energy generated. In which case, energy per threshold as a function of percentage total energy may be more comparable. For percentage distribution of energy within each sample site (**Table 2**), 466°C_{MRFT} and 705°C_{MRFT} indicate a higher percentage of energy generated below 300°C. Contrasting this, 592°C_{MRFT}

TABLE 2 | Table highlighting the total energy generated within each prescribed fire site, related to key thresholds in mortality (>50°C), charcoalification (>300°C), and flaming combustion (>400°C). These values have also been presented as percentages of total energy output exceeding mortality thresholds. All values are derived approximately from the calculated area under time-temperature curves (**Figure 4**) and reported to three significant figures.

Sample Set		466°C$_{MRFT}$	592°C$_{MRFT}$	705°C$_{MRFT}$	803°C$_{MRFT}$
Total energy expended (>50°C)		**29200**	**29100**	**44500**	**40900**
Energy Expended (°C)	50–299°C	15700	11800	23400	14200
	300–399°C	5480	4010	6130	6130
	>400°C	8060	13300	15000	20600
	Total < 300°C	15700	11800	23400	14200
	Total > 300°C	13500	17300	21200	26800
Percentage	50–299°C	53.7	40.5	52.5	34.6
Energy Expended (%)	300–399°C	18.8	13.8	13.8	15.0
	>400°C	27.6	45.7	33.8	50.4
	Total < 300°C	53.7	40.5	52.5	34.6
	Total > 300°C	46.3	59.5	47.5	65.4

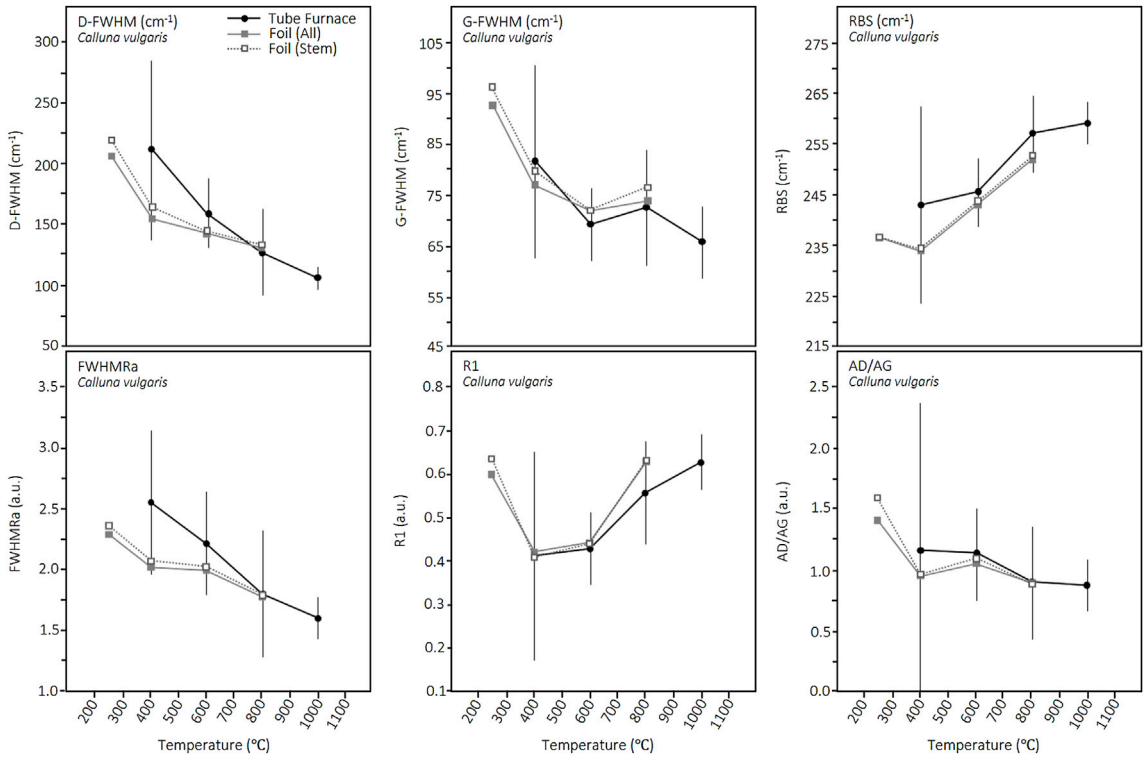

FIGURE 5 | Crossplots indicating the relationship between median Raman parameter values and the formation temperature of charcoals derived from foil (Theurer et al., 2021) and tube furnace pyrolysis (*this study*), respectively. Each data point represents median values from 150 individual spectral deconvolutions, with standard deviation for tube furnace charcoals shown by vertical black lines. Key in the top left crossplot corresponds to all succeeding plots. Here, "*foil (stem)*" and "*foil (all)*" refer to the sole use of *Calluna* stem, or collective stem, flower, and root data, respectively.

and 803°C$_{MRFT}$ appear to have generated more energy in exceedance of 300°C. The presentation of higher Raman-geothermometric temperatures calculated from samples at 592°C$_{MRFT}$ and 803°C$_{MRFT}$, and lower values in 466°C$_{MRFT}$ and 705°C$_{MRFT}$ (**Figure 4**), correspond directly to this difference in proportion of energy generated before and after 300°C. Simply, the greater proportion of total energy produced by each fire system above 300°C, the higher the calculated geothermometric temperature. This, in turn, equates to lower median FWHMRa values and consequent thermal maturity. It is worth noting, however, that the consideration of energy within a wildfire system in this instance is limited to approximating its impact on the maturation of microstructure. Characterizing a fire's intensity using energy output must otherwise include assessments of duration and heating rate (**Table 1**) for risk of equating sustained low temperature and rapid high temperature fire regimes.

4 DISCUSSION

4.1 The Influence of Reference Pyrolysis

With the intention of assessing the influence of pyrolysis methodology on resultant Raman parameter relationships, results presented here (tube-furnace pyrolysis) have been compared to established parameter trends. These have been derived from prior research into the foil-based pyrolysis of *Calluna* across natural wildfire temperatures, and the associated process of microstructural reorganization in charcoals (Theurer et al., 2021). Key differences in trend include variable presentation of identifiable charcoalification, and an overall reduction in thermal maturity of tube furnace charcoals, relative to those generated in foil at any given temperature (**Figure 5**).

Initial consideration of these inconsistencies may suggest them as a product of innate variabilities in origin material—though notably derived from a single species. It is, however, more likely that the observed differences in microstructural change with temperature result not from key procedural differences - given the consistency in method between studies—but rather, differences in heat application due to equipment and processes. Tube furnace equipment may be considered a more "modern" and reliable form of laboratory pyrolysis—guaranteeing flame retardation *via* the use of inert gas flow, without the possible limitations of foil thermal conductivity. However, the evidence of poorer microstructural development with temperature compared to foil pyrolysis experiments remains present. This could be considered the result of two possible influences; 1) tube furnace experiments detailed in this study fail to implement sufficient thermal energy to the sample, or 2) charcoals derived from foil pyrolysis underwent greater heating than expected. These sources of error suggest the potential for inert gas flow drawing heat from the surface of the sample, or localised uncontrolled flaming as a result of pyrolytic limitations, respectively. The limitation of pyrolysis yields, and greater removal of pyrolytic volatiles, has been observed under high nitrogen flow during experimental pyrolysis of jute (Choudhury et al., 2014) and palm oil biomass waste (Mohamed et al., 2013). Whilst this suggests the opportunity for similar removal of pyrolyzate and heat from the surface of charring plant material, the impact on charcoal yield with relation to flow rate shows no significant trend (Mohamed et al., 2013).

This difference in the degree of maturation presented by both methodologies remains particularly pertinent, given differences in the minimum temperature at which spectral evidence of charcoalification is presented. The lower observed limit of charcoalification has been previously reported at ~250°C (Jones et al., 1991), consistent with reported limits of hemi-/cellulose decomposition (Graham et al., 1984; Mohan et al., 2006). This is contrasted in recent studies reporting cellulose decomposition initiation closer to 280–290°C (Braadbaart et al., 2009; Scott, 2010). Chemical changes in organic matter during charcoalification may begin at lower temperatures, however the wood-charcoal transition has been observed between 310 and 370°C (Braadbaart and Poole, 2008), with full charcoalification occurring at 400°C (Vaughan and Nichols, 1995; Scott, 2010), accompanied by full aromatization (Braadbaart et al., 2009). This is, however, dependent on the characterization of "full charcoalification", as changes in mass, carbon content, biochemistry, structure, and reflectance continue up to, and exceed, 1200°C (Braadbaart and Poole, 2008; Braadbaart et al., 2009). More specifically, the generation of true charcoal may be associated with the occurrence of cell wall homogenization within the cellular structure of plant material, the temperatures associated with this process varying widely between 280 and 350°C (Scott et al., 2000; McParland et al., 2007; Scott, 2010; Osterkamp et al., 2018). It is below this threshold of ~300°C that presents significant variability in reflectance, particularly between species (Scott, 1989), indicating a key difficulty for the application of reflectance geothermometry during early charcoalification (McParland et al., 2007).

For foil pyrolysis, few Raman spectra of significant resolution were reported at 250°C (Theurer et al., 2021). Nonetheless, D- and G-bands were sufficient enough for deconvolution. This is contrasted by the lack of identifiable bands in spectra at 250°C using the tube furnace, suggesting significant differences in the application, transfer and/or permeation of the heating regime. Given the identical permeation and dwell times applied to all samples across both methodologies, we may confidently propose that the observed differences are the result of key contrasts in the thermal capabilities of the equipment used. Whilst no charcoal is reportable at 250°C for tube furnace pyrolysis, the more developed nature of spectra at 400°C suggests the lower limit of charcoalification for tube furnace pyrolysis exists between 250 and 400°C. This is consistent with natural limits of decomposition and charcoalification previously stated, though this remains dependent on the component material under analysis (Graham et al., 1984; Mohan et al., 2006). This further supports the explanation that the "simple" nature of foil pyrolysis may result in poor replication of anoxia, particularly at lower temperatures - as indicated by the similarities in parameter values after 400°C. This in turn may result in the generation of a flame and localised instances of a higher temperature than experimentally set.

4.2 Comparing Experimental and Modern Fire Thermometry

The discrepancy listed above, between recorded flame temperatures in a prescribed heathland fire and those calculated from microstructure using Raman FWHMRa, may be answered by considering the behavior of each fire system. The pattern described previously shows that charcoals formed during lower recorded temperatures of 466 and 592°C_{MRFT} exhibit greater calculated temperatures from Raman geothermometry relative to expected (**Figure 4**). The reverse is true for samples collected from 705 to 803°C_{MRFT}. Considering, first, the nature of the lower temperature samples, 466°C_{MRFT} presents a greater number of high-FWHMRa outlying data (comparable to 705°C_{MRFT}) which may reflect the incapability of lower

temperature fire regimes to consistently and fully char fuels. This would in turn present poorly developed Raman spectra, and associated width ratio values. Such an effect may be accentuated by the lower cooling rate in 466°C_{MRFT} and an extended duration of heating overall, offering a greater opportunity to partially-char material, or indeed extend the maturation of charcoals beyond expected values. This may be characterized by the post-flaming oxidation of charcoals as pyrolyzate depletes, namely "smouldering combustion" (Rein, 2013 *as cited in*; Belcher and Hudspith, 2016b). However, this is inconsistent with the nature of the fire regime recorded at 592°C_{MRFT}. These samples indicate the lowest duration of heating overall, accompanied by rapid heating and cooling - more consistent with reduced opportunity for maturation. Instead, samples from this site have generated the greatest calculated temperature from median FWHMRa (739°C). It is possible that the rapid nature of this heating regime presented more obvious and complete charcoalification, resulting in focused sampling and spectral acquisition, i.e., fewer data associated with lower temperature charcoalification. When considering the approximate total energy within each system (**Table 2**), both 466 and 592°C_{MRFT} present very similar total energy output (over 50°C). However, 592°C_{MRFT} exhibits a greater proportion of energy above 300°C, compared to 466°C_{MRFT} which expends most energy below 300°C, consistent with a less intense application of energy, heat, and microstructural maturation. This may explain why 592°C_{MRFT} samples present a microstructure consistent with greater thermal maturation than those at 466°C_{MRFT}.

For samples generated within a maximum of 705 and 803°C_{MRFT}, higher recorded temperatures are characterized by calculated temperatures lower than expected. Curiously, 705°C_{MRFT} reports the greatest heating duration, slowest cooling rate (**Table 1**) and greatest total energy expended over time (**Table 2**). This would be expected to generate a charcoal microstructure associated with greater maturity, and therefore greater calculated temperature through FWHMRa geothermometry. In contrast, these samples have generated the lowest median calculated temperature of all four fire systems (583°C). This may be explained by very rapid heating, reducing the opportunity for heating of fuel prior to ignition. Pre-ignition heating of fuels from a flame front, whilst intermittent and seldom reaching 350°C (Finney et al., 2015), promotes wood decomposition and generation of pyrolyzate, resulting in the creation of charcoal (Belcher and Hudspith, 2016b). Pre-ignition heating within smouldering fires similarly generates lower temperatures, approximating 80–100°C (Rein et al., 2008). Reduced pre-ignition heating would therefore result in reduced production and maturation of charcoal prior to ignition, and a larger proportion of energy expended for evaporation of fuel moisture, permitting ignition. A slow cooling rate may have also resulted in partial charring of material—as with 466°C_{MRFT}—generating instances of poor, highly variable charcoal microstructure and likewise spectral results. This is supported by the presence of numerous outlying data at very low maturity (high FWHMRa), and a greater proportion of total energy for this system expended below the 300°C. In contrast, samples at 803°C_{MRFT} underwent a short duration of heating and rapid cooling, potentially offering less time overall to mature the sample microstructure. This is somewhat complicated, however, by the presentation of high total energy, most of which occurred above 300°C. This would be expected to generate much higher temperatures than associated with the median FWHMRa value of this sample set, however it may explain why it remains the second highest calculated temperature.

It appears that in some instances there are consistencies between the microstructure present, and the behavior of energy flux within each system. This remains coherent with key recent findings in charcoal microstructural change, with specific reference to reflectance studies. Whilst charcoal reflectance analyses initially utilized oven-based pyrolysis to replicate the wildfire charcoalification process, much research has now deemed this form of replication inapplicable. The core principle behind this remains that oven-charring does not present the variable nature of heat and, most importantly, energy flux that occurs over the course of charcoalification in a natural wildfire (Belcher and Hudspith, 2016b; Hudspith and Belcher, 2017; Belcher et al., 2018). There are three key components of combustion within a fire: pyrolysis, flaming combustion, and oxidation or "smouldering combustion" of fuels (Belcher and Hudspith, 2016b). Oven-charring replicates the pyrolysis process solely, often with significant pre-heating of fuels, yet neglects the process of oxidation which has been shown to mature charcoal reflectance past that which is associated with peak heat intensity (Rein, 2013 *as cited in*; Belcher and Hudspith, 2016b). This "overprinting" of maturity has been directly observed, with results in Belcher et al. (2018) showing a 22% increase in reflectance from oven-pyrolyzed charcoals compared to those sourced from a natural-fire-replicative calorimetry process. These discrepancies are similarly reflected in cellular structures, indicating an inability of oven-charring to generate fracturing of the middle lamellae and distortion associated with the oxidizing component of smouldering combustion (Belcher and Hudspith, 2016b; Hudspith and Belcher 2017; Belcher et al., 2018). It becomes increasingly evident then, that microstructure within charcoals is not solely reliant on maximum temperature of formation, but rather a combination of combustion behavior and its relation to the dynamism of energy within a fire system.

The importance of energy application to microstructural change in charcoals is similarly reflected in applications of FTIR to charcoal thermometry. Statistical modelling, including multivariate and model-based clustering study, alongside FTIR applications has highlighted key associations between FTIR spectra and pyrolysis intensity (Gosling et al., 2019; Maezumi et al., 2021). A similar relationship has also been derived respective of charred species and temperatures experienced (Maezumi et al., 2021). The accuracy of these models, though generally good, remains somewhat limited. Reduced accuracy is particularly evident in low temperature classification, attributed to species-specific variability in chemistry, and the role this plays in altering structural development in early charcoalification (Maezumi et al., 2021). This effect is lessened by introducing broader allowances for error in temperature estimation (Gosling et al., 2019; Maezumi et al., 2021), though this raises questions as

to the potential influence variable temperature and energy flux may play in further limiting FTIR thermometry (Maezumi et al., 2021). Nevertheless, FTIR has proven consistently effective at estimating pyrolysis intensity *via* broad temperature-associated intensity classifications (i.e., low, moderate, high) with considerable potential in palaeofire assessment (Gosling et al., 2019; Constantine et al., 2021; Maezumi et al., 2021). Measured consideration for the influence of energy within a fire system is presented in Constantine et al. (2021) through their application of FTIR in understanding charring intensity. Charring intensity, here, refers to the quantification of fire intensity by considering energy output (°C) as a function of time. This is regarded as a more robust reflection of fire behavior and intensity (Constantine et al., 2021 *and references therein*), and corresponds to the application of similar considerations within this study. A strong correlation found within regression modelling in Constantine et al. (2021) suggests a close relationship between modelled and observed charring intensity—though limited to temperatures below 700°C. This conclusion, though somewhat disparate from the results presented here, still remains reliant on a methodology that replicates pyrolysis in a furnace. Consistency in expected and observed charring intensity may therefore reflect, simply, the consistency observed in thermal application within furnaces, as iterated in Belcher et al. (2018). This research does, however, promote a vital consideration of energy and time when developing microstructurally derived thermometry. This continues to suggest the need for further comparative research into charcoal thermometry techniques and the influence of energy in natural fire systems. Such research may come to require an understanding of the role of activation energy.

Via the study of charcoalified wood within pyroclastic deposits, Sawada et al. (2000) has shown that, through the assessment of activation energy, the reduction in charcoal hydrogen/carbon ratio (H/C) with maturation is increased with a simultaneous reduction in cooling rate. This is directly attributable to charcoal maturation under increasing temperature. The degree to which cooling rates influence resultant maturation are also relative to initial maximum emplacement temperatures (Sawada et al., 2000), indicating a further dimension to issues of accuracy in geothermometry when relying on microstructural change. For the spontaneous combustion of wood, component proportions (e.g., cellulose) related to material age have been shown to directly influence activation energy and resultant burning rates (Zachar et al., 2021). Furthermore, the concept of maturation in organic matter and activation energy has been a key consideration of historic source rock evaluation, linked directly to changes in reflectance as a function of temperature and time (e.g., Burnham and Sweeney, 1989). This is noteworthy given the similarities between charcoal and vitrinite reflectance in core principle, and by extension, Raman spectroscopy of organic carbon. It is clear that the nature of charcoal microstructure and geothermometry is related not only to maximum heat and associated energy, but also the way in which energy changes over time, its relation to the process of combustion, and the properties of fuels themselves.

The overall lack of one significant, definable influencing factor upon microstructural change suggests that the relationship between recorded temperature and Raman-derived microstructure is a function of many interacting factors, operating simultaneously. These factors, as we have identified, include the influence of energy flux within each sample site, however, additional potential factors may be divided into two further groups: natural, and methodological variability. The present study relies on the assumption that the temperature recorded by thermocouples is equal to that which is represented or expected by microstructural analysis of charcoals. This in itself may be subject to small differences in the ability for heat to permeate into fuels, whilst the accuracy of thermocouples may too be brought into question. It is more likely, however, that whilst samples were sourced from *Calluna* as close as possible to the relevant thermocouples, fire temperature and energy flux vary considerably within three-dimensions. This variability is likely to occur at a fine scale of resolution, as a function of the intermittent, turbulent, and convective nature of heat flow within a fire front (Finney et al., 2015), in turn resulting in considerably different temperatures experienced by fuels within a short distance of one another. This may explain the inconsistency between expected (recorded) flame temperatures, and temperatures of formation calculated from Raman geothermometry.

As for natural influences, the variability of charcoal microstructure as a result of differences in cellulose, lignin and hemicellulose proportions within plant material has been investigated previously using Raman (Ishimaru et al., 2007a). The influence of high lignin aromaticity on elevating charcoal reflectance has also been reported (Scott, 1989). Moisture content, typically removed from laboratory experiments, may too introduce a limiting factor on charcoal maturation, as a key determinant of fuel flammability (Belcher and Hudspith, 2016b). Greater moisture content within plant material requires a greater amount of energy to pyrolyze (Hudspith and Belcher, 2017). Belcher and Hudspith (2016b) also noted that microstructural change is strongly influenced by varying conditions of fuel moisture, with experimental results indicating significantly lower charcoal reflectance values at 70% moisture, compared to those charcoals produced at 7 and 0%.

Localised variations in air circulation and humidity, closely linked to vegetational moisture, may play a role in influencing the discrepancy between recorded flame and charring temperatures, due to fire limitative moisture and promotive air flow, respectively. These meteorological components have been linked closely to the increase in fire weather observed, and predicted to occur, with changes in anthropogenic climate (Jolly et al., 2015). However, the degree of variation occurring within centimeters, between thermocouple and sample, are likely negligible or indefinable. Ultimately, difficulty arises when attempting to infer potential influences within an unregulated and natural fire system at both macro- and microscopic scales.

4.3 Taphonomic Implications for Palaeowildfire Geothermometry

When considering the reflection of fire behavior in palaeocharcoals, a myriad of further additional biases and

potential impactors become apparent. These influences may be characterized by their occurrence as pre-, syn-, or post-fire effects, and are broadly associated with the concept of charcoal taphonomy.

A primary control on the nature of the charcoal record may be understood as production biases during the wildfire event itself—limited primarily by the temperatures generated and experienced. High severity fires indicate a tendency to produce smaller charcoal fraction sizes (Mastrolonardo et al., 2017), increasing the likelihood of depositional dilution, loss, and/or degradation post-fire—marked also, in part, as a function of fuel bulk density (Hudspith et al., 2018). Whilst fragment number is not considered a function of temperature, it has been associated more closely with variability between species, their density, and its relationship to constituent cell structure (Chrzazvez et al., 2014). Coarser fractions, commonly associated with wood fuels (Scott et al., 2000), have also shown instances of increased reflectance due to low microstructural amorphosity and sustained combustion (Mastrolonardo et al., 2017). This highlights not only the impact of fire temperature on fractionation and preservation of fuels, but indeed the influence of the fuels themselves in constraining charcoal production—with direct geothermometric implications. This is consistent with the pre-fire alteration of wood biochemistry *via* fungal and microbial decay retaining lignin-rich cellular structures (Blanchette, 2000; Schwarze, 2007; Hudspith and Belcher, 2017) and subsequently presenting heightened charcoal reflectance values post-charcoalification (Guo and Bustin, 1998; Hudspith and Belcher, 2017).

In fact, non-altered vegetation, too, shows an innate ability to limit charcoal-geothermometric applications. This is seen in the significant lignin-defined variability between tissue components within a single plant, and the resultant increase in reflectance values at a given temperature in lignified tissues, relative to less-lignified material (Scott, 1989; Guo and Bustin, 1998). Such influences are contrasted only by the influence of structural density in fuels (Braadbaart and Poole, 2008). This component-species level variability is also seen in charcoal transport and waterlogging; as species and bulk density (Nichols et al., 2000; Scott et al., 2000), water speed, salinity, and surface tension-limiting objects (Vaughan and Nichols, 1995) all play a role in the settling and deposition rates of charcoalified material. Aside from these influences, temperature-dependent fracturing within the plant microstructure acts to elevate permeability and subsequent charcoal settling rates (Vaughan and Nichols, 1995; Nichols et al., 2000). Considering, therefore, that the depositional rate of charcoals is as a result of temperature-induced structural variability, it is likely that different temperatures may be determined from geothermometry depending on the locality of deposition and distance from source.

For charcoals held or deposited terrestrially, high aromaticity due to high temperatures of formation (e.g., Ascough et al., 2008), contributes not only toward microstructural maturation but subsequent increases in charcoal stability and resistance to oxidative degradation (Ascough et al., 2018; Constantine and Mooney, 2021), growing increasingly susceptible with time and exposure (Ascough et al., 2011a; Ascough et al., 2020; Smidt et al., 2020), particularly in alkaline environments (Braadbaart et al., 2009; Ascough et al., 2011b). This suggests that low-temperature charcoals are in turn more susceptible to alteration, degradation, and preferential loss from the palaeofire record, including as a result of sample acquisition and analysis (Constantine and Mooney, 2021). Further removal of wildfire evidence may be perpetuated by subsequent fires—an effect proportional to fire temperature (Doerr et al., 2018). Here, surviving charcoals are likely to undergo further charcoalification and maturation relative to original fire conditions, reducing further their susceptibility to degradation, in turn preferentially preserving erroneously matured material. Such degradation of amorphous microstructural components may be contrasted by rapid deposition (Ascough et al., 2020), however this introduces a further dimension to the consideration of temperature-dependent waterlogging rates.

It is clear then that, whilst fire has a direct influence over the nature of charcoal microstructure and its presentation in the charcoal record; material, species, and ecosystem-level variabilities in fuel biochemistry have a direct influence in turn on the behavior of fire. Taken together, these factors can result in the preferential creation, transport, deposition, and degradation of wildfire-derived charcoals and make it challenging to accurately reconstruct post-fire temperatures.

5 CONCLUSION

Experimental observations, and the application of Raman band-width ratio geothermometry to heathland fire charcoals, have yielded the following key findings:

1) The method of pyrolysis implemented during the creation of reference charcoals contributes significantly towards the alteration of established spectral trends.
2) The D- and G-band width ratio (FWHMRa) records the most linear response to temperature for both furnace-based pyrolysis methodologies.
3) Temperatures derived from the Raman spectroscopy of heathland fire charcoals register differences to those directly recorded using thermocouples.
4) Analysing combustive energy, as a function of temperature change, cannot solely determine subsequent changes in charcoal microstructure.
5) Environmental factors and their innate natural variabilities are likely contributors to the continued difficulties experienced in temperature-specific geothermometry.

Further research is required to better assess how microstructural change is reflective of energy flux within variable fire conditions, and the ability of existing thermometry methods to disentangle this. Raman spectroscopy, in this instance, offers a unique opportunity to assess carbon-specific maturation features through the characterization of multi-faceted spectral features. Non-linear spectral changes, associated with the Raman analysis of

variable conditions of carbon maturation, may indeed be better suited to unravelling complex energy flux in natural fire systems.

Nevertheless, the consistency in Raman FWHMRa trends with increasing charring temperature, reiterated here, shows a continued applicability and reliability of this method when quantifying changes in wildfire activity—past and present.

DATA AVAILABILITY STATEMENT

The datasets presented in this study can be found in online repositories. The names of the repository/repositories and accession number(s) can be found below: https://doi.org/10.5281/zenodo.5746958 (Zenodo Repository).

AUTHOR CONTRIBUTIONS

TT, DMU, DJ, and DMA all contributed significantly toward the conception and design of this project. With regards to the specific conception, design, and conduct of prescribed fire methodology, NN was the sole contributor. NN collected wildfire charcoal samples and fire temperature (thermocouple) data. TT conducted experimental pyrolysis, as well as collection and processing of all spectroscopic data, and subsequent statistical analysis. The manuscript and figures were drafted by TT, with specific assistance from NN with regards to the prescribed fire methodology. All authors contributed toward the editing and revision of the manuscript and have approved the final version for submission.

FUNDING

Experimental pyrolysis, Raman spectroscopy and open access publication fees were all supported by funds from the University of Aberdeen School of Geosciences. Organization, generation, and collection of samples during prescribed heathland fire fieldwork was supported by the Macaulay Development Trust Studentship.

ACKNOWLEDGMENTS

We would like to thank Abbie McLaughlin, Sacha Fop, and Struan Simpson (Department of Chemistry, University of Aberdeen) unreservedly for their provision and assistance in the application of *Lenton* tube furnace equipment. Our sincerest thanks to Donald Barrie (Farm Manager, James Hutton Institute Glensaugh Research Farm) for his help in organizing and managing the prescribed heathland fires. We would also like to thank Sarah Woodin, Louise Ross (School of Biological Sciences, University of Aberdeen) and Alison Hester (James Hutton Institute) for providing guidance throughout this project, and to Robin Pakeman (James Hutton Institute) for guidance and editorial comments with regards to this article.

SUPPLEMENTARY MATERIAL

The Supplementary Material for this article can be found online at: https://www.frontiersin.org/articles/10.3389/feart.2022.827933/full#supplementary-material

REFERENCES

Ascough, P. L., Bird, M. I., Wormald, P., Snape, C. E., and Apperley, D. (2008). Influence of Production Variables and Starting Material on Charcoal Stable Isotopic and Molecular Characteristics. *Geochimica Cosmochimica Acta* 72 (24), 6090–6102. doi:10.1016/j.gca.2008.10.009

Ascough, P. L., Bird, M. I., Scott, A. C., Collinson, M. E., Cohen-Ofri, I., Snape, C. E., et al. (2010). Charcoal Reflectance Measurements: Implications for Structural Characterization and Assessment of Diagenetic Alteration. *J. Archaeol. Sci.* 37 (7), 1590–1599. doi:10.1016/j.jas.2010.01.020

Ascough, P. L., Bird, M. I., Francis, S. M., Thornton, B., Midwood, A. J., Scott, A. C., et al. (2011a). Variability in Oxidative Degradation of Charcoal: Influence of Production Conditions and Environmental Exposure. *Geochimica Cosmochimica Acta* 75 (9), 2361–2378. doi:10.1016/j.gca.2011.02.002

Ascough, P. L., Bird, M. I., Francis, S. M., and Lebl, T. (2011b). Alkali Extraction of Archaeological and Geological Charcoal: Evidence for Diagenetic Degradation and Formation of Humic Acids. *J. Archaeol. Sci.* 38 (1), 69–78. doi:10.1016/J.JAS.2010.08.011

Ascough, P. L., Bird, M. I., Meredith, W., Snape, C., Large, D., Tilston, E., et al. (2018). Dynamics of Charcoal Alteration in a Tropical Biome: A Biochar-Based Study. *Front. Earth Sci.* 6, 61. doi:10.3389/feart.2018.00061

Ascough, P. L., Brock, F., Collinson, M. E., Painter, J. D., Lane, D. W., and Bird, M. I. (2020). Chemical Characteristics of Macroscopic Pyrogenic Carbon Following Millennial-Scale Environmental Exposure. *Front. Environ. Sci.* 7, 203. doi:10.3389/fenvs.2019.00203

Belcher, C. M., and Hudspith, V. A. (2016a). Changes to Cretaceous Surface Fire Behaviour Influenced the Spread of the Early Angiosperms. *New Phytol.* 213 (3), 1521–1532. doi:10.1111/nph.14264

Belcher, C. M., and Hudspith, V. A. (2016b). The Formation of Charcoal Reflectance and its Potential Use in Post-fire Assessments. *Int. J. Wildland Fire* 25 (7), 775. doi:10.1071/WF15185

Belcher, C. M., Mander, L., Rein, G., Jervis, F. X., Haworth, M., Hesselbo, S. P., et al. (2010). Increased Fire Activity at the Triassic/Jurassic Boundary in Greenland Due to Climate-Driven Floral Change. *Nat. Geosci.* 3 (6), 426–429. doi:10.1038/ngeo871

Belcher, C. M., New, S. L., Santín, C., Doerr, S. H., Dewhirst, R. A., Grosvenor, M. J., et al. (2018). What Can Charcoal Reflectance Tell Us about Energy Release in Wildfires and the Properties of Pyrogenic Carbon? *Front. Earth Sci.* 6. doi:10.3389/feart.2018.00169

Belcher, C. M., New, S. L., Gallagher, M. R., Grosvenor, M. J., Clark, K., and Skowronski, N. S. (2021). Bark Charcoal Reflectance May Have the Potential to Estimate the Heat Delivered to Tree Boles by Wildland Fires. *Int. J. Wildland Fire* 30, 391–397. doi:10.1071/WF20071

Benicio, J. R. W., Jasper, A., Spiekermann, R., Garavaglia, L., Pires-Oliveira, E. F., Machado, N. T. G., et al. (2019). Recurrent Palaeo-Wildfires in a Cisuralian Coal Seam: A Palaeobotanical View on High-Inertinite Coals from the Lower Permian of the Paraná Basin, Brazil. *PLoS ONE* 14 (3), e0213854. doi:10.1371/journal.pone.0213854

Beny-Bassez, C., and Rouzaud, J.-N. (1985). Characterization of Carbonaceous Materials by Correlated Electron and Optical Microscopy and Raman Microspectroscopy. *Scanning Electron Microsc.* 1985 (1), 119–132.

Beyssac, O., Goffé, B., Chopin, C., and Rouzaud, J. N. (2002). Raman Spectra of Carbonaceous Material in Metasediments: a New Geothermometer. *J. Metamorph. Geol.* 20 (9), 859–871. doi:10.1046/j.1525-1314.2002.00408.x

Blanchette, R. A. (2000). A Review of Microbial Deterioration Found in Archaeological Wood from Different Environments. *Int. Biodeterior. Biodegrad.* 46 (3), 189–204. doi:10.1016/S0964-8305(00)00077-9

Braadbaart, F., and Poole, I. (2008). Morphological, Chemical and Physical Changes during Charcoalification of Wood and its Relevance to Archaeological Contexts. *J. Archaeol. Sci.* 35 (9), 2434–2445. doi:10.1016/j.jas.2008.03.016

Braadbaart, F., Poole, I., and Van Brussel, A. A. (2009). Preservation Potential of Charcoal in Alkaline Environments: an Experimental Approach and Implications for the Archaeological Record. *J. Archaeol. Sci.* 36, 1672–1679. doi:10.1016/j.jas.2009.03.006

Burnham, A. K., and Sweeney, J. J. (1989). A Chemical Kinetic Model of Vitrinite Maturation and Reflectance. *Geochimica Cosmochimica Acta* 53 (10), 2649–2657. doi:10.1016/0016-7037(89)90136-1

Choudhury, N. D., Chutia, R. S., Bhaskar, T., and Kataki, R. (2014). Pyrolysis of Jute Dust: Effect of Reaction Parameters and Analysis of Products. *J. Mater Cycles Waste Manag.* 16, 449–459. doi:10.1007/s10163-014-0268-4

Chrzazvez, J., Théry-Parisot, I., Fiorucci, G., Terral, J.-F., and Thibaut, B. (2014). Impact of Post-depositional Processes on Charcoal Fragmentation and Archaeobotanical Implications: Experimental Approach Combining Charcoal Analysis and Biomechanics. *J. Archaeol. Sci.* 44, 30–42. doi:10.1016/j.jas.2014.01.006

Cohen-Ofri, I., Weiner, L., Boaretto, E., Mintz, G., and Weiner, S. (2006). Modern and Fossil Charcoal: Aspects of Structure and Diagenesis. *J. Archaeol. Sci.* 33 (3), 428–439. doi:10.1016/j.jas.2005.08.008

Collinson, M. E., Steart, D. C., Scott, A. C., Glasspool, I. J., and Hooker, J. J. (2007). Episodic Fire, Runoff and Deposition at the Palaeocene-Eocene Boundary. *J. Geol. Soc.* 164 (1), 87–97. doi:10.1144/0016-76492005-185

Collinson, M. E., Steart, D. C., Harrington, G. J., Hooker, J. J., Scott, A. C., Allen, L. O., et al. (2009). Palynological Evidence of Vegetation Dynamics in Response to Palaeoenvironmental Change across the Onset of the Paleocene-Eocene Thermal Maximum at Cobham, Southern England. *Grana* 48 (1), 38–66. doi:10.1080/00173130802707980

Constantine, M., and Mooney, S. (2021). Widely Used Charcoal Analysis Method in Paleo Studies Involving NaOCl Results in Loss of Charcoal Formed below 400°C. *Holocene*, 095968362110417. doi:10.1177/09596836211041740

Constantine, M., Mooney, S., Hibbert, B., Marjo, C., Bird, M., Cohen, T., et al. (2021). Using Charcoal, ATR FTIR and Chemometrics to Model the Intensity of Pyrolysis: Exploratory Steps towards Characterising Fire Events. *Sci. Total Environ.* 783, 147052. doi:10.1016/j.scitotenv.2021.147052

de Sousa, D. V., Guimarães, L. M., Félix, J. F., Ker, J. C., Schaefer, C. E. R. G., and Rodet, M. J. (2020). Dynamic of the Structural Alteration of Biochar in Ancient Anthrosol over a Long Timescale by Raman Spectroscopy. *PLoS One* 15 (3), e0229447. doi:10.1371/journal.pone.0229447

Deldicque, D., and Rouzaud, J.-N. (2020). Temperatures reached by the roof structure of Notre-Dame de Paris in the fire of April 15th 2019 determined by Raman paleothermometry. *Comptes Rendus Géoscience* 352 (1), 7–18. doi:10.5802/crgeos.9

Deldicque, D., Rouzaud, J.-N., and Velde, B. (2016). A Raman - HRTEM Study of the Carbonization of Wood: A New Raman-Based Paleothermometer Dedicated to Archaeometry. *Carbon* 102, 319–329. doi:10.1016/j.carbon.2016.02.042

Denis, E. H., Pedentchouk, N., Schouten, S., Pagani, M., and Freeman, K. H. (2017). Fire and Ecosystem Change in the Arctic across the Paleocene-Eocene Thermal Maximum. *Earth Planet. Sci. Lett.* 467, 149–156. doi:10.1016/j.epsl.2017.03.021

Doerr, S. H., Santín, C., Merino, A., Belcher, C. M., and Baxter, G. (2018). Fire as a Removal Mechanism of Pyrogenic Carbon from the Environment: Effects of Fire and Pyrogenic Carbon Characteristics. *Front. Earth Sci.* 6. doi:10.3389/feart.2018.00127

Edwards, D., and Axe, L. (2004). Anatomical Evidence in the Detection of the Earliest Wildfires. *PALAIOS* 19 (2), 113–128. doi:10.1669/0883-1351(2004)019<0113:aeitdo>2.0.co;2

Ferrari, A. C., and Robertson, J. (2000). Interpretation of Raman Spectra of Disordered and Amorphous Carbon. *Phys. Rev. B* 61 (20), 14095–14107. doi:10.1103/PhysRevB.61.14095

Finney, M. A., Cohen, J. D., Forthofer, J. M., McAllister, S. S., Gollner, M. J., Gorham, D. J., et al. (2015). Role of Buoyant Flame Dynamics in Wildfire Spread. *Proc. Natl. Acad. Sci. U.S.A.* 112 (32), 9833–9838. doi:10.1073/pnas.1504498112

Glasspool, I. J., Edwards, D., and Axe, L. (2004). Charcoal in the Silurian as Evidence for the Earliest Wildfire. *Geol* 32 (5), 381–383. doi:10.1130/G20363.1

Glasspool, I. J., Edwards, D., and Axe, L. (2006). Charcoal in the Early Devonian: A Wildfire-Derived Konservat-Lagerstätte. *Rev. Palaeobot. Palynology* 142 (3-4), 131–136. doi:10.1016/j.revpalbo.2006.03.021

Gosling, W. D., Cornelissen, H. L., and McMichael, C. N. H. (2019). Reconstructing Past Fire Temperatures from Ancient Charcoal Material. *Palaeogeogr. Palaeoclimatol. Palaeoecol.* 520, 128–137. doi:10.1016/j.palaeo.2019.01.029

Graham, R. G., Bergougnou, M. A., and Overend, R. P. (1984). Fast Pyrolysis of Biomass. *J. Anal. Appl. Pyrolysis* 6 (2), 95–135. doi:10.1016/0165-2370(84)80008-X

Guedes, A., Valentim, B., Prieto, A. C., Rodrigues, S., and Noronha, F. (2010). Micro-Raman Spectroscopy of Collotelinite, Fusinite and Macrinite. *Int. J. Coal Geol.* 83 (4), 415–422. doi:10.1016/j.coal.2010.06.002

Guo, Y., and Bustin, R. M. (1998). FTIR Spectroscopy and Reflectance of Modern Charcoals and Fungal Decayed Woods: Implications for Studies of Inertinite in Coals. *Int. J. Coal Geol.* 37 (1–2), 29–53. doi:10.1016/S0166-5162(98)00019-6

Harris, T. M. (1958). Forest Fire in the Mesozoicfire in the Mesozoic. *J. Ecol.* 46, 447–453. doi:10.2307/2257405

Henry, D. G., Jarvis, I., Gillmore, G., Stephenson, M., and Emmings, J. F. (2018). Assessing Low-Maturity Organic Matter in Shales Using Raman Spectroscopy: Effects of Sample Preparation and Operating Procedure. *Int. J. Coal Geol.* 191, 135–151. doi:10.1016/j.coal.2018.03.005

Henry, D. G., Jarvis, I., Gillmore, G., and Stephenson, M. (2019a). A Rapid Method for Determining Organic Matter Maturity Using Raman Spectroscopy: Application to Carboniferous Organic-Rich Mudstones and Coals. *Int. J. Coal Geol.* 203, 87–98. doi:10.1016/j.coal.2019.01.003

Henry, D. G., Jarvis, I., Gillmore, G., and Stephenson, M. (2019b). Raman Spectroscopy as a Tool to Determine the Thermal Maturity of Organic Matter: Application to Sedimentary, Metamorphic and Structural Geology. *Earth-Science Rev.* 198, 102936. doi:10.1016/j.earscirev.2019.102936

Hudspith, V. A., and Belcher, C. M. (2017). Observations of the Structural Changes that Occur during Charcoalification: Implications for Identifying Charcoal in the Fossil Record. *Palaeontology* 60, 503–510. doi:10.1111/pala.12304

Hudspith, V. A., Belcher, C. M., Kelly, R., and Hu, F. S. (2015). Charcoal Reflectance Reveals Early Holocene Boreal Deciduous Forests Burned at High Intensities. *PLoS ONE* 10 (4), e0120835. doi:10.1371/journal.pone.0120835

Hudspith, V. A., Hadden, R. M., Bartlett, A. I., and Belcher, C. M. (2018). Does Fuel Type Influence the Amount of Charcoal Produced in Wildfires? Implications for the Fossil Record. *Palaeontology* 61, 159–171. doi:10.1111/pala.12341

IPCC (2021). *Climate Change 2021: The Physical Science Basis. Contribution of Working Group I to the Sixth Assessment Report of the Intergovernmental Panel on Climate Change*. Editors V. Masson-Delmotte, P. Zhai, A. Pirani, S. L. Connors, C. Péan, S. Berger, et al. (Cambridge, New York: Cambridge University Press). *In Press*.

Ishimaru, K., Hata, T., Bronsveld, P., Meier, D., and Imamura, Y. (2007a). Spectroscopic Analysis of Carbonization Behavior of Wood, Cellulose and Lignin. *J. Mater Sci.* 42, 122–129. doi:10.1007/s10853-006-1042-3

Ishimaru, K., Hata, T., Bronsveld, P., Nishizawa, T., and Imamura, Y. (2007b). Characterization of Sp2- and Sp3-Bonded Carbon in Wood Charcoal. *J. Wood Sci.* 53, 442–448. doi:10.1007/s10086-007-0879-7

Jasper, A., Guerra-Sommer, M., Abu Hamad, A. M. B., Bamford, M., Bernardes-de-Oliveira, M. E. C., Tewari, R., et al. (2013). The Burning of Gondwana: Permian Fires on the Southern Continent-A Palaeobotanical Approach. *Gondwana Res.* 24 (1), 148–160. doi:10.1016/j.gr.2012.08.017

Jolly, W. M., Cochrane, M. A., Freeborn, P. H., Holden, Z. A., Brown, T. J., Williamson, G. J., et al. (2015). Climate-induced Variations in Global Wildfire Danger from 1979 to 2013. *Nat. Commun.* 6 (7537). doi:10.1038/ncomms8537

Jones, T. P., Scott, A. C., and Cope, M. (1991). Reflectance Measurements and the Temperature of Formation of Modern Charcoals and Implications for Studies of Fusain. *Bull. – Soc. Geol. Fr.* 162, 193–200.

Kawakami, M., Karato, T., Takenaka, T., and Yokoyama, S. (2005). Structure Analysis of Coke, Wood Charcoal and Bamboo Charcoal by Raman Spectroscopy and Their Reaction Rate with CO2. *ISIJ Int.* 45 (7), 1027–1034. doi:10.2355/isijinternational.45.1027

Keeley, J. E., and Rundel, P. W. (2005). Fire and the Miocene Expansion of C4 Grasslands. *Ecol. Lett.* 8 (7), 683–690. doi:10.1111/j.1461-0248.2005.00767.x

Keeley, J. E. (2009). Fire Intensity, Fire Severity and Burn Severity: A Brief Review and Suggested Usage. *Int. J. Wildland Fire* 18, 116–126. doi:10.1071/WF07049

Korasidis, V. A., Wallace, M. W., Wagstaff, B. E., Holdgate, G. R., Tosolini, A.-M. P., and Jansen, B. (2016). Cyclic Floral Succession and Fire in a Cenozoic Wetland/peatland System. *Palaeogeogr. Palaeoclimatol. Palaeoecol.* 461, 237–252. doi:10.1016/j.palaeo.2016.08.030

Maezumi, S. Y., Gosling, W. D., Kirschner, J., Chevalier, M., Cornelissen, H. L., Heinecke, T., et al. (2021). A Modern Analogue Matching Approach to Characterize Fire Temperatures and Plant Species from Charcoal. *Palaeogeogr. Palaeoclimatol. Palaeoecol.* 578, 110580. doi:10.1016/j.palaeo.2021.110580

Manabe, T., Ohata, M., Yoshizawa, S., Nakajima, D., Goto, S., Uchida, K., et al. (2007). Effect of Carbonization Temperature on the Physicochemical Structure of Wood Charcoal. *Trans. Mat. Res. Soc. Jpn.* 32 (4), 1035–1038. doi:10.14723/tmrsj.32.1035

Marlon, J. R., Bartlein, P. J., Daniau, A.-L., Harrison, S. P., Maezumi, S. Y., Power, M. J., et al. (2013). Global Biomass Burning: a Synthesis and Review of Holocene Paleofire Records and Their Controls. *Quat. Sci. Rev.* 65, 5–25. doi:10.1016/j.quascirev.2012.11.029

Marynowski, L., and Simoneit, B. R. T. (2009). Widespread Upper Triassic to Lower Jurassic Wildfire Records from Poland: Evidence from Charcoal and Pyrolytic Polycyclic Aromatic Hydrocarbons. *PALAIOS* 24 (12), 785–798. doi:10.2110/palo.2009.p09-044r

Mastrolonardo, G., Hudspith, V. A., Francioso, O., Rumpel, C., Montecchio, D., Doerr, S. H., et al. (2017). Size Fractionation as a Tool for Separating Charcoal of Different Fuel Source and Recalcitrance in the Wildfire Ash Layer. *Sci. Total Environ.* 595, 461–471. doi:10.1016/j.scitotenv.2017.03.295

Mauquoy, D., Payne, R. J., Babeshko, K. V., Bartlett, R., Boomer, I., Bowey, H., et al. (2020). Falkland Island Peatland Development Processes and the Pervasive Presence of Fire. *Quat. Sci. Rev.* 240, 106391. doi:10.1016/j.quascirev.2020.106391

McInerney, F. A., and Wing, S. L. (2011). The Paleocene-Eocene Thermal Maximum: A Perturbation of Carbon Cycle, Climate, and Biosphere with Implications for the Future. *Annu. Rev. Earth Planet. Sci.* 39 (1), 489–516. doi:10.1146/annurev-earth-040610-133431

McParland, L. C., Collinson, M. E., Scott, A. C., Steart, D. C., Grassineau, N. V., and Gibbons, S. J. (2007). Ferns and Fires: Experimental Charring of Ferns Compared to Wood and Implications for Paleobiology, Paleoecology, Coal Petrology, and Isotope Geochemistry. *PALAIOS* 22, 528–538. doi:10.2110/palo.2005.p05-138r

Mohamed, A. R., Hamzah, Z., Daud, M. Z. M., and Zakaria, Z. (2013). The Effects of Holding Time and the Sweeping Nitrogen Gas Flowrates on the Pyrolysis of EFB Using a Fixed-Bed Reactor. *Procedia Eng.* 53, 185–191. doi:10.1016/j.proeng.2013.02.024

Mohan, D., Pittman, C. U., and Steele, P. H. (2006). Pyrolysis of Wood/biomass for Bio-Oil: A Critical Review. *Energy fuels..* 20 (3), 848–889. doi:10.1021/ef0502397

Nabbefeld, B., Grice, K., Summons, R. E., Hays, L. E., and Cao, C. (2010). Significance of Polycyclic Aromatic Hydrocarbons (PAHs) in Permian/Triassic Boundary Sections. *Appl. Geochem.* 25 (9), 1374–1382. doi:10.1016/j.apgeochem.2010.06.008

New, S. L., Hudspith, V. A., and Belcher, C. M. (2018). Quantitative Charcoal Reflectance Measurements Better Link to Regrowth Potential Than Ground-Based Fire-Severity Assessments Following a Recent Heathland Wildfire at Carn Brea, Cornwall, UK. *Int. J. Wildland Fire* 27, 845–850. doi:10.1071/WF18112

Nichols, G., and Jones, T. (1992). Fusain in Carboniferous Shallow Marine Sediments, Donegal, Ireland: The Sedimentological Effects of Wildfire. *Sedimentology* 39, 487–502. doi:10.1111/j.1365-3091.1992.tb02129.x

Nichols, G. J., Cripps, J. A., Collinson, M. E., and Scott, A. C. (2000). Experiments in Waterlogging and Sedimentology of Charcoal: Results and Implications. *Palaeogeogr. Palaeoclimatol. Palaeoecol.* 164 (1–4), 43–56. doi:10.1016/S0031-0182(00)00174-7

Orvis, K. H., Lane, C. S., and Horn, S. P. (2005). Laboratory Production of Vouchered Reference Charcoal from Small Wood Samples and Non-woody Plant Tissues. *Palynology* 29, 1–11. doi:10.1080/01916122.2005.9989601

Osterkamp, I. C., Lara, D. M. d., Gonçalves, T. A. P., Kauffmann, M., Périco, E., Stülp, S., et al. (2018). Changes of Wood Anatomical Characters of Selected Species of Araucaria- during Artificial Charring - Implications for Palaeontology. *Acta Bot. Bras.* 32, 198–211. doi:10.1590/0102-33062017abb0360

Paris, O., Zollfrank, C., and Zickler, G. A. (2005). Decomposition and Carbonisation of Wood Biopolymers-A Microstructural Study of Softwood Pyrolysis. *Carbon* 43 (1), 53–66. doi:10.1016/j.carbon.2004.08.034

Petersen, H. I., and Lindström, S. (2012). Synchronous Wildfire Activity Rise and Mire Deforestation at the Triassic-Jurassic Boundary. *PLoS ONE* 7 (10), e47236. doi:10.1371/journal.pone.0047236

Phillips, N., and Nogrady, B. (2020). The Race to Decipher How Climate Change Influenced Australia's Record Fires. *Nature* 577, 610–612. doi:10.1038/d41586-020-00173-7

Potgieter-Vermaak, S., Maledi, N., Wagner, N., Van Heerden, J. H. P., Van Grieken, R., and Potgieter, J. H. (2011). Raman Spectroscopy for the Analysis of Coal: a Review. *J. Raman Spectrosc.* 42 (2), 123–129. doi:10.1002/jrs.2636

Pyne, S. (2015). The Fire Age' [online]. Aeon. Available at: https://aeon.co/essays/how-humans-made-fire-and-fire-made-us-human (Accessed on January 29th, 2021).

Rein, G., Cleaver, N., Ashton, C., Pironi, P., and Torero, J. L. (2008). The Severity of Smouldering Peat Fires and Damage to the Forest Soil. *Catena* 74 (3), 304–309. doi:10.1016/j.catena.2008.05.008

Rein, G. (2013). "Smouldering Fires and Natural Fuels," in *Fire Phenomena and the Earth System: An Interdisciplinary Guide to Fire Science*. Editor C. M. Belcher (Oxford, UK: John Wiley & Sons), 15–33. doi:10.1002/9781118529539.ch2

Rimmer, S. M., Hawkins, S. J., Scott, A. C., and Cressler, W. L. (2015). The Rise of Fire: Fossil Charcoal in Late Devonian Marine Shales as an Indicator of Expanding Terrestrial Ecosystems, Fire, and Atmospheric Change. *Am. J. Sci.* 315 (8), 713–733. doi:10.2475/08.2015.01

Rouzaud, J.-N., Deldicque, D., Charon, É., and Pageot, J. (2015). Carbons at the Heart of Questions on Energy and Environment: A Nanostructural Approach. *Comptes Rendus Geosci.* 347 (3), 124–133. doi:10.1016/j.crte.2015.04.004

Sawada, Y., Sampei, Y., Hyodo, M., Yagami, T., and Fukue, M. (2000). Estimation of Emplacement Temperatures of Pyroclastic Flows Using H/C Ratios of Carbonized Wood. *J. Volcanol. Geotherm. Res.* 104, 1–20. doi:10.1016/S0377-0273(00)00196-7

Schwarze, F. W. M. R. (2007). Wood Decay under the Microscope. *Fungal Biol. Rev.* 21, 133–170. doi:10.1016/j.fbr.2007.09.001

Scott, A. C., and Damblon, F. (2010). Charcoal: Taphonomy and Significance in Geology, Botany and Archaeology. *Palaeogeogr. Palaeoclimatol. Palaeoecol.* 291 (1-2), 1–10. doi:10.1016/j.palaeo.2010.03.044

Scott, A. C., and Glasspool, I. J. (2005). Charcoal Reflectance as a Proxy for the Emplacement Temperature of Pyroclastic Flow Deposits. *Geol* 33 (7), 589–592. doi:10.1130/G21474.1

Scott, A. C., and Jones, T. (1994). The Nature and Influence of Fire in Carboniferous Ecosystems. *Palaeogeogr. Palaeoclimatol. Palaeoecol.* 106 (1-4), 91–112. doi:10.1016/0031-0182(94)90005-1

Scott, A. C., Cripps, J. A., Collinson, M. E., and Nichols, G. J. (2000). The Taphonomy of Charcoal Following a Recent Heathland Fire and Some Implications for the Interpretation of Fossil Charcoal Deposits. *Palaeogeogr. Palaeoclimatol. Palaeoecol.* 164 (1–4), 1–31. doi:10.1016/S0031-0182(00)00168-1

Scott, A. C. (1989). Observations on the Nature and Origin of Fusain. International Journal of Coal. *Geology* 12 (1-4), 443–475. doi:10.1016/0166-5162(89)90061-X

Scott, A. C. (2000). The Pre-quaternary History of Fire. *Palaeogeogr. Palaeoclimatol. Palaeoecol.* 164 (1-4), 281–329. doi:10.1016/S0031-0182(00)00192-9

Scott, A. C. (2010). Charcoal Recognition, Taphonomy and Uses in Palaeoenvironmental Analysis. *Palaeogeogr. Palaeoclimatol. Palaeoecol.* 291 (1-2), 11–39. doi:10.1016/j.palaeo.2009.12.012

Smidt, E., Tintner, J., Nelle, O., Oliveira, R. R., Patzlaff, R., Novotny, E. H., et al. (2020). Infrared Spectroscopy Refines Chronological Assessment, Depositional Environment and Pyrolysis Conditions of Archeological Charcoals. *Sci. Rep.* 10, 12427. doi:10.1038/s41598-020-69445-6

Theurer, T., Muirhead, D. K., Jolley, D., and Mauquoy, D. (2021). The Applicability of Raman Spectroscopy in the Assessment of Palaeowildfire Intensity. *Palaeogeogr. Palaeoclimatol. Palaeoecol.* 570, 110363. doi:10.1016/j.palaeo.2021.110363

Tuinstra, F., and Koenig, J. L. (1970). Raman Spectrum of Graphite. *J. Chem. Phys.* 53 (3), 1126–1130. doi:10.1063/1.1674108

Vaughan, A., and Nichols, G. (1995). Controls on the Deposition of Charcoal: Implications for Sedimentary Accumulations of Fusain. *J. Sediment. Res.* 65 (1a), 129–135. doi:10.1306/D426804A-2B26-11D7-8648000102C1865D

Wilkins, R. W. T., Boudou, R., Sherwood, N., and Xiao, X. (2014). Thermal Maturity Evaluation from Inertinites by Raman Spectroscopy: The 'RaMM' Technique. *Int. J. Coal Geol.* 128-129, 143–152. doi:10.1016/j.coal.2014.03.006

Wilkins, R. W. T., Wang, M., Gan, H., and Li, Z. (2015). A RaMM Study of Thermal Maturity of Dispersed Organic Matter in Marine Source Rocks. *Int. J. Coal Geol.* 150-151, 252–264. doi:10.1016/j.coal.2015.09.007

Wilkins, R. W. T., Sherwood, N., and Li, Z. (2018). RaMM (Raman Maturity Method) Study of Samples Used in an Interlaboratory Exercise on a Standard Test Method for Determination of Vitrinite Reflectance on Dispersed Organic Matter in Rocks. *Mar. Petroleum Geol.* 91, 236–250. doi:10.1016/j.marpetgeo.2017.12.030

Wopenka, B., and Pasteris, J. D. (1993). Structural Characterization of Kerogens to Granulite-Facies Graphite: Applicability of Raman Microprobe Spectroscopy. *Am. Mineralogist* 78 (5-6), 533–557.

Yamauchi, S., and Kurimoto, Y. (2003). Raman Spectroscopic Study on Pyrolyzed Wood and Bark of Japanese Cedar: Temperature Dependence of Raman Parameters. *J. Wood Sci.* 49, 235–240. doi:10.1007/s10086-002-0462-1

Yamauchi, S., Kikuchi, Y., and Kurimoto, Y. (2000). Raman Spectral Changes of Sugi Bark during Thermal Degradation and Carbonization. *J. Soc. Mater. Sci. Jpn.* 49, 227–228. doi:10.2472/jsms.49.9Appendix_227

Zachar, M., Čabalová, I., Kačíková, D., and Jurczyková, T. (2021). Effect of Natural Aging on Oak Wood Fire Resistance. *Polymers* 13 (13), 2059. doi:10.3390/polym13132059

Zakrzewski, A., Kosakowski, P., Waliczek, M., and Kowalski, A. (2020). Polycyclic Aromatic Hydrocarbons in Middle Jurassic Sediments of the Polish Basin Provide Evidence for High-Temperature Palaeo-Wildfires. *Org. Geochem.* 145, 104037. doi:10.1016/j.orggeochem.2020.104037

Zhang, Z., Wang, C., Lv, D., Hay, W. W., Wang, T., and Cao, S. (2020). Precession-scale Climate Forcing of Peatland Wildfires during the Early Middle Jurassic Greenhouse Period. *Glob. Planet. Change* 184, 103051. doi:10.1016/j.gloplacha.2019.103051

Zhou, B., Shen, C., Sun, W., Bird, M., Ma, W., Taylor, D., et al. (2014). Late Pliocene-Pleistocene Expansion of C4 Vegetation in Semiarid East Asia Linked to Increased Burning. *Geology* 42 (12), 1067–1070. doi:10.1130/G36110.1

Zickler, G. A., Smarsly, B., Gierlinger, N., Peterlik, H., and Paris, O. (2006). A Reconsideration of the Relationship between the Crystallite Size La of Carbons Determined by X-Ray Diffraction and Raman Spectroscopy. *Carbon* 44 (15), 3239–3246. doi:10.1016/j.carbon.2006.06.029

Conflict of Interest: The authors declare that the research was conducted in the absence of any commercial or financial relationships that could be construed as a potential conflict of interest.

Publisher's Note: All claims expressed in this article are solely those of the authors and do not necessarily represent those of their affiliated organizations, or those of the publisher, the editors and the reviewers. Any product that may be evaluated in this article, or claim that may be made by its manufacturer, is not guaranteed or endorsed by the publisher.